Submitted to ***Geophysical Research Letters***

Asymmetric Responses of the Western Tropical Pacific Sea Level to El Niño and La Niña

Qiuping Ren[1,2], Yuanlong Li[1,3,4], Fei Zheng[3,5], Fan Wang[1,2,3,4,*], Jing Duan[1,3,4]

[1]Key Laboratory of Ocean Circulation and Waves, Institute of Oceanology, Chinese Academy of Sciences, Qingdao, China,
[2]University of Chinese Academy of Sciences, Beijing, China,
[3]Center for Ocean Mega-Science, Chinese Academy of Sciences, Qingdao, China,
[4]Function Laboratory for Ocean Dynamics and Climate, Qingdao National Laboratory for Marine Science and Technology, Qingdao, China,
[5]International Center for Climate and Environment Science, Institute of Atmospheric Physics, Chinese Academy of Sciences, Beijing, China,

April 2020

[*]**Corresponding Author:**

Fan Wang

Key Laboratory of Ocean Circulation and Waves, Institute of Oceanology, Chinese Academy of Sciences, Qingdao 266071, China.
Email: fwang@qdio.ac.cn

Key Points.

1） The responses of the western tropical Pacific sea level to ENSO are obviously asymmetric, and the response to El Niño is evidently stronger.

2） The different surface wind anomaly structure between El Niño and La Niña is critical for the asymmetric response of sea level.

3） The asymmetric ocean responses to ENSO may contribute to the ENSO asymmetry.

Abstract

The western tropical Pacific (WTP) exhibits large interannual sea level anomalies (SLAs), and the sea level falling in El Niño is evidently stronger than the rising in La Niña. The asymmetry is most prominent near 160°E with the response to El Niño larger by three times and becomes less obvious near the western boundary. Sensitivity experiments of a simplified ocean model suggest that the asymmetry in surface wind forcing structure between El Niño and La Niña is critical. The El Niño's westerly wind anomaly patch locates more east than the La Niña's easterly wind patch during the mature stage, and its upwelling effects are accumulated over a wider longitude range and cause stronger negative SLAs in the WTP. Near the western boundary, however, upwelling effects are attenuated by easterly wind anomalies during El Niño conditions. The asymmetric ocean responses to ENSO winds may participate in the asymmetry of ENSO cycle.

Plain Language Summary

ENSO is the most influential climate variability mode of the Pacific and causes strong interannual sea level anomalies (SLAs) in the western tropical Pacific (WTP). We notice that the WTP's sea level falling in El Niño condition is stronger than its sea level rising in La Niña. This difference is most prominent near 160°E, where the falling in El Niño is stronger by three times. This phenomenon becomes much less evident near the western boundary of the Pacific basin. We find that the difference in surface wind anomaly structures between El Niño and La Niña is the primary cause. El Niño's westerly wind anomaly center locates more east than La Niña's easterly

wind anomaly center in their mature phase, and there are easterly wind anomalies emerging near the western boundary during El Niño. Therefore, effect of El Niño's westerly wind anomaly is accumulated over a wider longitude range and causes stronger sea level falling in the WTP. But this effect becomes weaker near the western boundary, due to easterly wind anomalies there. By contrast, effect of La Niña's easterly wind anomaly strengthens monotonically from east to west, but the produced sea level rising signatures are mainly confined to the WTP.

Keywords

Western Tropical Pacific, Sea Level, ENSO, ENSO asymmetry, Interannual Variability

1. Introduction

Regional sea level change, as an essential aspect of climate change, is attracting increasing attention of scientific communities and the general public, because of its threats on eco-systems and people of coastal residence (e.g., Nicholls & Cazenave, 2010; Cazenave & Cozannet, 2014). There is a paramount demand for improved understanding of regional sea level changes on various timescales (e.g., Milne et al., 2009; Church et al., 2013; Stammer et al., 2013). Sea level changes over the tropical Pacific Ocean are particularly pronounced on interannual timescale, as largely modulated by El Niño-Southern Oscillation (ENSO) (e.g., Cazenave et al., 2008; Antonov et al., 2005; Cheng et al., 2008). It is evident in Figure 1a that the western tropical Pacific (WTP) shows stronger interannual sea level anomalies (SLAs) than other regions, as quantified the standard deviation of low-passed SLAs. The WTP shows strong sea level rising (falling) during the La Niña (El Niño) condition, as a result of prevailing easterly (westerly) wind anomalies over the tropical Pacific basin (Wyrtki, 1975; Zebiak, 1984; Alory & Delcroix, 2002; Gu & Li, 2009; Nerem et al., 2010; Merrifield, 2011; Zhang & Church, 2012; Chang et al., 2013; Becker et al., 2016; Hamlington et al., 2016; Wang, 2018). The sea level rising during La Niña conditions is expected to aggravate coastal erosion, extreme marine flooding, or saltwater intrusion in coastal aquifers (Nicholls & Tol, 2006; Nicholls et al., 2007; Nicholls & Cazenave, 2010), thus becomes a major threat for the densely populated coastal regions. However, the sea level falling during El Niño causes the coral reef exposure and could damage the region’s ecosystem. There are many heavily-populated coasts and islands in the WTP, so the sea level changes during ENSO are well worth studying.

El Niño and La Niña are, however, not mirrors of each other. They exhibit obvious asymmetry in magnitude, duration time, and occurrence frequency (e.g., Yu et al., 1997; Burgers & Stephenson, 1999; Ohba & Ueda, 2007; Gergis & Fowler, 2009; An & Choi, 2009; Okumura & Deser, 2010). Their signatures on sea level are also asymmetric, owing to not only ENSO's asymmetry but also the nonlinearity in ocean response (Niedzielski & Kosek, 2010; Swierczynska et al., 2013; Im et al., 2015; An & Kim, 2017). Previous studies have demonstrated that ENSO asymmetry is contributed by nonlinear dynamical heating of ocean current advection (e.g., Kang & Kug, 2002; Jin et al., 2003; An & Jin, 2004; Su et al., 2010). As dynamically associated with the upper-ocean currents through pressure gradient, the asymmetric SLAs induced by ENSO may affect ocean current advection of heat and thereby participate in the ENSO asymmetry.

In this study, we aim to investigate the asymmetric response of the WTP sea level to ENSO and the underlying dynamical processes. This effort is of paramount need for the prediction and projection of regional sea level change and adaptions of the low-lying coasts and islands, as well as for understanding the dynamics of ENSO asymmetry. The rest of the paper is structured as follows. Section 2 describes the data and models. Section 3 describes the asymmetric SLAs of the WTP in response to ENSO. Section 4 explores the underlying dynamics through a simplified ocean model. Section 5 presents concluding remarks.

2. Data and Models

2.1. Data

In this study we use 0.25° × 0.25°, monthly satellite SLA data of 1993-2016 from Archiving Validation, and Interpretation of Satellite Oceanography (AVISO; Le Traon et al., 1998) and sea level records of three tidal gauge stations in the WTP: Malakal at 7.33°N, 134.45°E for 1979-2016, Kapingamrangi at 1.1°N, 154.78°E for 1929-2016, and Lombrum at 2.04°S, 147.47°E for 1995-2016 (Figure S1 in the Supporting Information). The Hadley Centre Sea Ice and Sea Surface Temperature (HadISST) data set (Kennedy et al., 2011) of the Met Office during 1979-2016 with horizontal resolution of 1° × 1° is used to compute Niño-3.4 index and identify El Niño and La Niña conditions. Surface winds and other surface atmospheric fields of 1979-2016 are taken from the 0.75° monthly dataset of the European Centre for Medium-Range Weather Forecasts (ECMWF) ERA-interim (Dee et al., 2011).

2.2. HYCOM

The HYbrid Coordinate Ocean Model (HYCOM) version 2.2.18 (Bleck, 2002) are used to simulate interannual SLAs in the tropical Pacific Ocean. HYCOM is configured to the Pacific Ocean basin between 48°S-48°N, 110°E-70°W, with a horizontal resolution of 1/3°×1/3° and 26 hybrid vertical layers (Li et al., 2015; Ren et al., 2020). Surface atmospheric forcing fields (winds, heat fluxes, precipitation, etc.) are taken from ERA-interim. Three sponge layers are applied to the western, southern and northern open-ocean boundaries, where model temperature and salinity are related to the World Ocean Atlas 2009 (WOA09) climatology (Antonov et al., 2010).

More details of model configuration are described in Ren et al. (2020). Subsequent to the spin-up run of 30 years under monthly climatologic forcing, two parallel experiments are performed under daily ERA-Interim fields for the period of 1979-2016. The control run (HYCOM-CTL) is forced with the original daily atmospheric fields and assumed to contain the complete processes. This experiment can well reproduce the amplitude and spatial distribution of interannual SLA and upper-ocean circulation variation in observation (Figure 1b; Ren et al., 2020). Another experiment, HYCOM-TAU, uses daily wind stress forcing as HYCOM-CTL, but all the other forcing fields (heat and freshwater fluxes) are fixed to monthly climatology. HYCOM-TAU is used to evaluate the effects of wind forcing on sea level.

2.3. Reduced-Gravity Ocean Model

To achieve more in-depth understanding, a series of experiments are performed with a 1.5-layer nonlinear reduced-gravity ocean (RGO) model. This model mainly represents the 1st-mode baroclinic response of the ocean to surface wind forcing, which is the dominant source of large-scale interannual variability in sea level and upper-ocean circulation of the WTP (e.g., Qiu & Chen, 2010, 2012). The model is configured to the Pacific Ocean basin between 40°S-40°N, 100°E-70°W with horizontal resolutions of 0.25°×0.25° and forced by monthly ERA-Interim surface winds. Readers are referred to Duan et al. (2019) for more details of the model configuration. After a spin-up of 10 years under climatological wind forcing, the control run of RGO model (RGO-CTL) is forced by realistic monthly winds. RGO model experiments (Table S1) are forced by idealized wind forcing to examine the role of wind forcing asymmetry and are described in Section 4.

3. Asymmetric Responses to El Niño and La Niña

To highlight the interannual variations associated with ENSO, we analyze the 13-month low-pass filtered anomaly fields with the monthly climatology removed. Skewness S is a measure of the distribution asymmetry with $S = 0$ indicating a normal distribution (White, 1980). Figure 1c shows the skewness of the observed SLA over the tropical Pacific for 1993-2016. The eastern tropical Pacific is positively skewed with the maximum S of ~2.0, while the central-western tropical Pacific is negatively skewed with the minimum S of -2.0 and a horseshoe structure extending from the equator to extratropical regions in both hemispheres. This distribution of SLA skewness resembles that of SST anomaly (An & Jin, 2004; Niedzielski & Kosek, 2010) and is likely associated with the positive skewness of ENSO (Nerem et al., 2010). The El Niño condition is characterized by positive SLAs in the eastern Pacific and negative SLAs in the WTP, and these anomalies are stronger in amplitude than the opposite SLAs occurring in La Niña condition (Niedzielski & Kosek, 2010; Figure S1).

In addition to the asymmetry residing in ENSO (e.g., as quantified by the skewness of Niño-3.4 index), the asymmetric responses of sea level to El Niño and La Niña also contribute to the SLA asymmetry shown in Figure 1c. We regress SLAs onto the normalized Niño-3.4 index separately for the El Niño condition (Niño-3.4 > 0) and the La Niña condition (Niño-3.4 < 0). The corresponding regression coefficients, namely k_{Nino} and k_{Nina}, are used to quantify the responses of SLA to El

Niño and La Niña, respectively (Figures 1d and 1e). The response time of sea level to ENSO shows spatial variation, as indicated by the lead-lag correlation (Figure S2a). For each grid point, the lead-lag time of the maximal correlation is used to compute the regression coefficient. The results are not dramatically different from those of simultaneous regression (Figure S2b). Figures 1d and 1e show distributions of k_{Nino} and k_{Nina}. In the WTP, the maximal k_{Nino} of ~-0.2 m is located 20°-30° away from the western boundary, and k_{Nino} decreases in magnitude as approaching the western boundary. By contrast, the peak k_{Nina} values of ~-0.15 m are close to the western boundary. We further use the ratio of k_{Nino} to k_{Nina} to quantify the response asymmetry,

$$R_k = \frac{k_{Nino}}{k_{Nina}}. \quad (1)$$

$R_k = 1$ denotes symmetric response of SLAs to El Niño and La Niña, while $R_k > 1$ and $R_k < 1$ indicates stronger and weaker response to El Niño than to La Niña, respectively. As shown in Figure 1f, R_k reaches the largest value near 160°E with values exceeding 3.0, indicating that the response of SLA to El Niño is stronger by at least 3 times than the response to La Niña. R_k is weakened to ~1.0 near the western boundary, implying SLA responses there are nearly symmetric. This interesting distribution of R_k in the WTP and underlying dynamics are worthy of systematic investigation. One may notice that R_k is < 1 in the central Pacific and is > 1 in the eastern Pacific, indicative of prevailing asymmetry over the tropical Pacific basin. In the following, we focus on explaining the R_k distribution in the WTP.

Simulations of HYCOM and RGO model have faithfully reproduced the observed interannual variations of sea level at three tidal gauge stations (Figure S3).

The upper-layer thickness (ULT) anomaly of the 1.5-layer RGO model is a good proxy of SLA in the tropical Pacific (e.g., Qiu & Chen, 2010, 2012; Chang et al., 2013; Duan et al., 2019). The correlations among AVISO, HYCOM-CTL, HYCOM-TAU and RGO-CTL at the three tidal gauge stations are all above 0.85. The asymmetric responses of SLAs to El Niño and La Niña in the WTP during 1993-2016 can be realistically reproduced by HYCOM-CTL, HYCOM-TAU, and RGO-CTL (Figures 2a-2c), although RGO-CTL fails to capture the features in the eastern Pacific. The good performance of HYCOM-TAU and RGO-CTL indicates that the interannual SLAs in the WTP and their asymmetric features are primarily the results of ENSO wind forcing, and the underlying dynamics can be explored by sensitive model experiments with prescribed wind forcing fields.

4. Dynamics

To include more ENSO events, we use the period of 1979-2016 to perform model experiments (Table S1), although R_k of 1979-2016 shows detailed differences from that of 1993-2016 in the northwest Pacific (Figures 2d-2f). According to existing studies of ENSO asymmetry, the different spatial and temporal characteristics of wind anomalies are essential to cause the SST asymmetry between El Niño and La Niña (Kang & Kug, 2002; An & Kim, 2017). To examine which aspect of ENSO's wind forcing is critical in regulating the asymmetric responses of SLAs, we adopt a statistical model based on the singular value decomposition (SVD) of wind stress and SST (Kang & Kug, 2000), which is expressed as

$$\boldsymbol{\tau}'\ (x,y,t) = \sum_{n}^{N} c(n)\left[\sum_{x,y} V_{\mathrm{SST}}(x,y,n) T(x,y,t)\right] V_{\tau}(x,y,n), \qquad (2)$$

where *x, y,* and *t* represent longitude, latitude, and time, respectively, V_{SST} and $V\tau$ are the SVD singular vectors for SST and wind stress, *T* is the SST anomaly field, and *n* = 1, 2, … , *N* indicates the *n*th mode of SVD, $\sum_{x,y}$ indicates spatial integration over the region of 100°-290°E, 40°S-40°N. *c*(*n*) represents the correlation between SST and wind stress anomalies,

$$c(n) = \frac{\sum_t t_{\mathrm{SST}}(t,n)\, t_{\tau}(t,n)}{\sum_t t_{\mathrm{SST}}(t,n)^2} \quad , \qquad (3)$$

where t_{SST} and $t\tau$ are the corresponding time series, the numerator is the covariance of t_{SST} and $t\tau$ and the denominator is the variance of t_{SST}, and $\sum_t$ indicates temporal integration from January 1979 to December 2016. Zonal and meridional components of $\boldsymbol{\tau}'$ are separately computed. All the RGO sensitive experiments are forced by monthly wind stress anomalies constructed by Eq. 2 (representing ENSO wind forcing) plus monthly climatological winds.

We first perform two experiments, namely EXP1 and EXP2. EXP1 uses different wind stress anomaly fields for El Niño and La Niña conditions. Specifically, $\boldsymbol{\tau}'_{\mathrm{Nino}}$ and $\boldsymbol{\tau}'_{\mathrm{Nina}}$ are reconstructed separated for Niño-3.4 ≥ 0 and Niño-3.4 < 0 conditions (Figures S4a and S4b) using Eq. 2, respectively, so that the synthesized $\boldsymbol{\tau}'$ still retains the difference in spatial structure between El Niño and La Niña conditions. By contrast, EXP2 does not distinguish El Niño and La Niña conditions and uses reconstructed $\boldsymbol{\tau}'$ for the entire model period (Figure S4c). As such, the difference between EXP1 and EXP2 represents the effect of different wind anomaly structures between El Niño and La Niña on SLAs. In EXP1 and EXP2, we use only the leading mode (*n* = 1) of SVD to reconstruct $\boldsymbol{\tau}'$ (Figure S4), which explains > 85% of the total covariance and mainly represents ENSO's mature phase (Figure S5). The higher SVD modes largely represent the transition stages between El Niño and La Niña polarities (Figure S5) and have limited impacts on the asymmetry of SLAs (Figure S6).

Figures 3a and 3b show R_k distributions of ULT produced by EXP1 and EXP2, respectively. EXP1 is able to reproduce large R_k values in the WTP as RGO-CTL, whereas R_k is generally close to 1.0 in EXP2. These results suggest that the asymmetry in surface wind structures between El Niño and La Niña is largely responsible for asymmetric responses of the WTP sea level. Note that EXP2 still retains some asymmetric characteristics of ENSO winds, such as the asymmetries in intensity, frequency, and temporal evolution. Figure 3b however indicates that these factors have little contributions to SLA asymmetry. This is confirmed by an additional experiment EXP3, which adopts an idealized sine time series for $\boldsymbol{\tau}'$ (Table S1) and achieves similar results to EXP2 (Figure S7).

In the equatorial zone, zonal component of wind stress τ^x is much more influential for the ocean than the meridional component. We repeat EXP1 and EXP2 using only τ^x anomaly, and τ^y is fixed to monthly climatology (EXP1-TAUX and EXP2-TAUX). The results of two experiments achieve are broadly consistent with EXP1 and EXP2 (Figures 3c and 3d). Therefore, the spatial structure of τ^x is critical for the asymmetric responses. The typical structures of ULT and τ^x in EXP1-TAUX for warm and cold phases are shown in Figures 3e and 3f, respectively, as represented by the leading SVD mode of τ^x and ULT. Notice that westerly wind anomaly patch of El Niño locates more east than the easterly wind anomaly patch of La Niña in their mature phase, and correspondingly the zero value of ULT anomaly of El Niño also locates more east (Jin, 1997; Kang & Kug, 2002). During El Niño there are easterly wind anomalies near the western boundary. The strong negative ULT anomalies in El Niño are seen over a wide longitude range and weaken as approaching the western boundary, while the positive ULT anomalies in La Niña are confined to the far WTP and generally strengthen westward.

To better elucidate how the wind forcing structure cause asymmetric SLAs, we show in Figure 4 the zonal distributions of τ^x and ULT in the equatorial band (5°S-5°N). It is clearly discernible in Figure 4a that the El Niño's westerly wind anomaly patch locates more east than the La Niña's easterly wind anomaly patch. The forcing effect of equatorial zonal wind stress on sea level and ULT slopes can be roughly expressed in a linear relationship (Sverdrup, 1947; McCreary, 1977; Alory & Delcroix, 2002; Palanisamy et al., 2014),

$$\frac{dh}{dx} = \tau^x, \tag{4}$$

where h is ULT anomaly or SLA. Therefore, $h(x)$ at a given longitude x can be determined by the integration of Eq. (4) from the eastern boundary x_E = 70°W along equator,

$$h(x) = h(x_E) + \int_{x_E}^{x} \tau^x \, dx. \tag{5}$$

Since $h(x_E)$ diffuses quickly away from the eastern boundary as free Rossby waves and has little impact on the interior Pacific (Qiu et al., 2013), $h(x)$ is primarily determined by the zonal integral of τ^x from x_E to x (second term). As such, the negative ULT anomaly in El Niño in the WTP is much stronger than the positive ULT anomaly in La Niña owing to the much wider westerly wind anomaly patch to its east. West of 160°E, easterly wind anomaly near the western boundary causes downwelling of the ocean, resulting in the attenuation of negative ULT anomalies there. By contrast, the La Niña's positive ULT anomalies are continuously strengthened by easterly wind anomalies. As a result, the ULT anomalies of El Niño and La Niña are comparable in amplitude in the far WTP, and the asymmetry of response is no longer evident there (right panel of Figure 4a). In EXP2-TAUX (Figure 4b), without the difference in wind forcing structure (left panel), the asymmetric responses cannot be reproduced (middle and right panels).

Figure 4c shows the zonal distributions of ULT anomaly and regression coefficients predicted by the linear theory, which compare favorably with Figure 4a. It indicates that the linear theory can to a large extent capture the processes causing asymmetric responses to ENSO winds and confirms the critical role played by the structure of zonal wind anomaly. Under this theoretical framework, the response asymmetry R_k can be theoretically expressed as,

$$R_k(x) \approx \frac{\int_{x_E}^{x} \tau^x{}_{Nino} dx}{\int_{x_E}^{x} \tau^x{}_{Nina} dx} \ , \tag{6}$$

where $\tau^x{}_{Nino}$ and $\tau^x{}_{Nina}$ are the zonal wind stress anomaly in El Niño and La Niña conditions, respectively. Eq. (6) clearly suggests the sensitivity of $R_k(x)$ to the distribution of τ^x from x to the eastern boundary.

5. Concluding Remarks

The WTP exhibits large interannual variations of sea level, and the sea level falling in El Niño is stronger than the rising in La Niña. Here we show that this asymmetry is most prominent near 160°E with the response to El Niño larger by ~3 times and becomes much less obvious near the western boundary. RGO model experiments suggest that the asymmetric surface wind anomaly structure between El Niño and La Niña conditions is critical. El Niño's westerly wind anomaly patch locates more east than La Niña's easterly wind anomaly patch in their mature stages. As such, the upwelling effects of westerly wind anomalies are accumulated over a wider longitude range and cause stronger negative SLAs in the WTP. As approaching further toward the western boundary, positive SLAs in La Niña continue to amplify, while negative SLAs of El Niño are attenuated by easterly wind anomalies in the far WTP.

Here we reveal the sensitivity of the asymmetric SLAs in the WTP to the ENSO wind structures. It is interesting to investigate whether the asymmetric SLAs in turn contributes to the ENSO asymmetry in amplitude and temporal evolutions. This can be investigated through careful heat budget analysis that evaluate the effects of asymmetric current advection on SST variability. In addition, the zonal surface wind patch dominates the SLA asymmetry along the equator, and its off-equatorial structure may affect the asymmetry beyond the equator by modifying the wind stress curl (An & Bong, 2016). In addition to wind forcing, the effects of local nonlinear processes, such as mesoscale eddies, on sea level in the WTP are not resolved by the RGO model experiments (Chen et al., 2015; Qiu et al., 2015), which can be also examined in the future study.

Acknowledgments

This research is supported by National Natural Science Foundation of China (grants 41730534 and 41806014) and the National Program on Global Change and Air-Sea Interaction (grant GASI-IPOVAI-01-01). AVISO sea level data are available at http://marine.copernicus.eu/services-portfolio/access-to-products/. Tidal gauges data are available at https://www.psmsl.org/. ERA-Interim wind data are available at https://apps.ecmwf.int/datasets/. HadISST data are downloaded from Met-Office website https://www.metoffice.gov.uk/hadobs/.

References

Alory, G., and T. Delcroix (2002), Interannual sea level changes and associated mass transports in the tropical Pacific from TOPEX/Poseidon data and linear model results (1964-1999), Journal of Geophysical Research-Oceans, 107(C10), doi: 10.1029/2001jc001067.

An, S. I., and F. F. Jin (2004), Nonlinearity and asymmetry of ENSO, Journal of Climate, 17(12), 2399-2412, doi: 10.1175/1520-0442(2004)017<2399:naaoe>2.0.co;2.

An, S.-I., and J. Choi (2009), Seasonal locking of the ENSO asymmetry and its influence on the seasonal cycle of the tropical eastern Pacific sea surface temperature, Atmospheric Research, 94(1), 3-9, doi: 10.1016/j.atmosres.2008.09.029.

An, S.-I., and H. Bong (2016), Inter-decadal change in El Nino-Southern Oscillation examined with Bjerknes stability index analysis, Climate Dynamics, 47(3-4), 967-979, doi: 10.1007/s00382-015-2883-8.

An, S.-I., and J.-W. Kim (2017), Role of nonlinear ocean dynamic response to wind on the asymmetrical transition of El Nino and La Nina, Geophysical Research Letters, 44(1), 393-400, doi: 10.1002/2016gl071971.

Antonov, J. I., S. Levitus, and T. P. Boyer (2005), Thermosteric sea level rise, 1955-2003, Geophysical Research Letters, 32(12), doi: 10.1029/2005gl023112.

Antonov, J., Seidov, D., Boyer, T., Locarnini, R., Mishonov, A., Garcia, H., et al. (2010). World ocean atlas 2009. In S. Levitus (Ed.), Salinity (Vol. 2, pp. 184).

Washington, DC: US Gov. Print. Off.Bleck, R. (2002), An oceanic general circulation model framed in hybrid isopycnic-Cartesian coordinates, Ocean Modelling, 4(1), 55-88, doi: 10.1016/s1463-5003(01)00012-9.

Becker, M., B. Meyssignac, C. Letetrel, W. Llovel, A. Cazenave, and T. Delcroix (2012), Sea level variations at tropical Pacific islands since 1950, Global and Planetary Change, 80-81, 85-98, doi: 10.1016/j.gloplacha.2011.09.004.

Burgers, G., and D. B. Stephenson (1999), The "normality" of El Nino, Geophysical Research Letters, 26(8), 1027-1030, doi: 10.1029/1999gl900161.

Cazenave, A., and G. Le Cozannet (2014), Sea level rise and its coastal impacts, Earths Future, 2(2), 15-34, doi: 10.1002/2013ef000188.

Cazenave, A., A. Lombard, and W. Llovel (2008), Present-day sea level rise: A synthesis, Comptes Rendus Geoscience, 340(11), 761-770, doi: 10.1016/j.crte.2008.07.008.

Chang, Y.-T., L. Du, S.-W. Zhang, and P.-F. Huang (2013), Sea level variations in the tropical Pacific Ocean during two types of recent El Nino events, Global and Planetary Change, 108, 119-127, doi: 10.1016/j.gloplacha.2013.06.001.

Chen, L., Y. Jia, and Q. Liu (2015), Mesoscale eddies in the Mindanao Dome region, Journal of Oceanography, 71(1), 133-140, doi: 10.1007/s10872-014-0255-3.

Cheng, X., Y. Qi, and W. Zhou (2008), Trends of sea level variations in the Indo-Pacific warm pool, Global and Planetary Change, 63(1), 57-66, doi: 10.1016/j.gloplacha.2008.06.001.

Church, J. A., et al. (2013), Sea-Level Rise by 2100, Science, 342(6165), 1445-1445, doi: 10.1126/science.342.6165.1445-a.

Dee, D. P., et al. (2011), The ERA-Interim reanalysis: configuration and performance of the data assimilation system, Quarterly Journal of the Royal Meteorological Society, 137(656), 553-597, doi: 10.1002/qj.828.

Duan, J., Y. Li, F. Wang, and Z. Chen (2019), Multidecadal Change of the Mindanao Current: Is There a Robust Trend?, Geophysical Research Letters, 46(12), 6755-6764, doi: 10.1029/2019gl083090.

Gergis, J. L., and A. M. Fowler (2009), A history of ENSO events since AD 1525: implications for future climate change, Climatic Change, 92(3-4), 343-387, doi: 10.1007/s10584-008-9476-z.

Xiao-li, G. U., and L. I. Pei-liang (2009), Pacific sea level variations and its factors, Acta Oceanologica Sinica, 31(1), 28-36.

Hamlington, B. D., S. H. Cheon, P. R. Thompson, M. A. Merrifield, R. S. Nerem, R. R. Leben, and K. Y. Kim (2016), An ongoing shift in Pacific Ocean sea level, Journal of Geophysical Research-Oceans, 121(7), 5084-5097, doi: 10.1002/2016jc011815.

Im, S.-H., S.-I. An, S. T. Kim, and F.-F. Jin (2015), Feedback processes responsible for El Nino-La Nina amplitude asymmetry, Geophysical Research Letters, 42(13), 5556-5563, doi: 10.1002/2015gl064853.

Jin, F. F. (1997), A theory of interdecadal climate variability of the North Pacific ocean-atmosphere system, Journal of Climate, 10(8), 1821-1835, doi: 10.1175/1520-0442(1997)010<1821:atoicv>2.0.co;2.

Jin, F. F., J. S. Kug, S. I. An, and I. S. Kang (2003), A near-annual coupled ocean-atmosphere mode in the equatorial Pacific ocean, Geophysical Research Letters, 30(2), doi: 10.1029/2002gl015983.

Kang, I. S., and J. S. Kug (2002), El Nino and La Nina sea surface temperature anomalies: Asymmetry characteristics associated with their wind stress anomalies, Journal of Geophysical Research-Atmospheres, 107(D19), doi: 10.1029/2001jd000393.

Kang, I. S., and J. S. Kug (2000), An El-Nino prediction system using an intermediate ocean and a statistical atmosphere, Geophysical Research Letters, 27(8), 1167-1170, doi: 10.1029/1999gl011023.

Kennedy, J. J., N. A. Rayner, R. O. Smith, D. E. Parker, and M. Saunby (2011), Reassessing biases and other uncertainties in sea surface temperature observations measured in situ since 1850: 2. Biases and homogenization, Journal of Geophysical Research-Atmospheres, 116, doi: 10.1029/2010jd015220.

Le Traon, P. Y., F. Nadal, and N. Ducet (1998), An improved mapping method of multisatellite altimeter data, Journal of Atmospheric and Oceanic Technology, 15(2), 522-534, doi: 10.1175/1520-0426(1998)015<0522:aimmom>2.0.co;2.

Li, Y., and W. Han (2015), Decadal Sea Level Variations in the Indian Ocean Investigated with HYCOM: Roles of Climate Modes, Ocean Internal Variability, and Stochastic Wind Forcing, Journal of Climate, 28(23), 9143-9165, doi: 10.1175/jcli-d-15-0252.1.

McCreary, J. (1976), Eastern Tropical Ocean Response to Changing Wind

System-with Application to El Nino, Journal of Physical Oceanography, 6(5), 632-645, doi: 10.1175/1520-0485(1976)006<0632:etortc>2.0.co;2.

Merrifield, M. A. (2011), A Shift in Western Tropical Pacific Sea Level Trends during the 1990s, Journal of Climate, 24(15), 4126-4138, doi: 10.1175/2011jcli3932.1.

Milne, G. A., W. R. Gehrels, C. W. Hughes, and M. E. Tamisiea (2009), Identifying the causes of sea-level change, Nature Geoscience, 2(7), 471-478, doi: 10.1038/ngeo544.

Nerem, R. S., D. P. Chambers, C. Choe, and G. T. Mitchum (2010), Estimating Mean Sea Level Change from the TOPEX and Jason Altimeter Missions, Marine Geodesy, 33, 435-446, doi: 10.1080/01490419.2010.491031.

Nicholls, R. J., and R. S. J. Tol (2006), Impacts and responses to sea-level rise: A global analysis of the SRES scenarios over the twenty-first century, Philos. Trans. R. Soc. A Math. Phys. Eng. Sci., 364(1841), 1073–1095, doi:10.1098/rsta-2006.1754.

Nicholls, R. J., P. P. Wong, V. R. Burkett, J. O. Codignotto, J. E. Hay, R. F. McLean, S. Ragoonaden, and C. D. Woodroffe (2007), Coastal systems and low-lying areas, in Climate Change 2007: Impacts, Adaptation and Vulnerability. Fourth Assessment Report of the Intergovernmental Panel on Climate Change (IPCC, 2007), edited by M. L. Parry, O. F. Canziani, J. P. Palutikof, P. J. van der Linden, and C. E. Hanson, Cambridge University Press, Cambridge, UK. pp. 315–356.

Nicholls, R. J., and A. Cazenave (2010), Sea-level rise and its impact on coastal zones (June, pg 1517, 2007), Science, 329(5992), 628-628.

Niedzielski, T., and W. Kosek (2010), El Nino's Impact on the Probability Distribution of Sea Level Anomaly Fields, Polish Journal of Environmental Studies, 19(3), 611-620.

Ohba, M., and H. Ueda (2007), An impact of SST anomalies in the Indian ocean in acceleration of the El Nino to La Nina transition, Journal of the Meteorological Society of Japan, 85(3), 335-348, doi: 10.2151/jmsj.85.335.

Okumura, Y. M., and C. Deser (2010), Asymmetry in the Duration of El Nino and La Nina, Journal of Climate, 23(21), 5826-5843, doi: 10.1175/2010jcli3592.1.

Qiu, B., and S. Chen (2010), Interannual-to-Decadal Variability in the Bifurcation of the North Equatorial Current off the Philippines, Journal of Physical Oceanography, 40(11), 2525-2538, doi: 10.1175/2010jpo4462.1.

Qiu, B., and S. Chen (2012), Multidecadal Sea Level and Gyre Circulation Variability in the Northwestern Tropical Pacific Ocean, Journal of Physical Oceanography, 42(1), 193-206, doi: 10.1175/jpo-d-11-061.1.

Qiu, B., S. Chen, and H. Sasaki (2013), Generation of the North Equatorial Undercurrent Jets by Triad Baroclinic Rossby Wave Interactions, Journal of Physical Oceanography, 43(12), 2682-2698, doi: 10.1175/jpo-d-13-099.1.

Qiu, B., S. Chen, L. Wu, and S. Kida (2015), Wind- versus Eddy-Forced Regional Sea Level Trends and Variability in the North Pacific Ocean, Journal of Climate, 28(4), 1561-1577, doi: 10.1175/jcli-d-14-00479.1.

Ren, Q., Y. Li, F. Wang, J. Duan, S. Hu, and F. Wang (2020), Variability of the Mindanao Current Induced by El Niño Events, Journal of Physical

Oceanography, 0(0), null, doi: 10.1175/jpo-d-19-0150.1.

Palanisamy, H., A. Cazenave, T. Delcroix, and B. Meyssignac (2015), Spatial trend patterns in the Pacific Ocean sea level during the altimetry era: the contribution of thermocline depth change and internal climate variability, Ocean Dynamics, 65(3), 341-356, doi: 10.1007/s10236-014-0805-7.

Stammer, D., A. Cazenave, R. M. Ponte, and M. E. Tamisiea (2013), Causes for Contemporary Regional Sea Level Changes, in Annual Review of Marine Science, Vol 5, edited by C. A. Carlson and S. J. Giovannoni, pp. 21-46.

Su, J., R. Zhang, T. Li, X. Rong, J. S. Kug, and C.-C. Hong (2010), Causes of the El Nino and La Nina Amplitude Asymmetry in the Equatorial Eastern Pacific, Journal of Climate, 23(3), 605-617, doi: 10.1175/2009jcli2894.1.

Sverdrup, H. U. (1947), NOTE ON THE CORRECTION OF REVERSING THERMOMETERS, Journal of Marine Research, 6(2), 136-138.

Wang, C. (2018), A review of ENSO theories, National Science Review, 5(6), 813-825, doi: 10.1093/nsr/nwy104.

Swerczynska, M., T. Niedzielski, and W. Kosek (2014), Semiannual and annual oscillations of sea level and their impact on asymmetry between El Nino and La Nina episodes, Studia Geophysica Et Geodaetica, 58(2), 302-325, doi: 10.1007/s11200-013-1124-z.

White, G. H. (1980), SKEWNESS, KURTOSIS AND EXTREME VALUES OF NORTHERN HEMISPHERE GEOPOTENTIAL HEIGHTS, Monthly Weather Review, 108(9), 1446-1455, doi:

10.1175/1520-0493(1980)108<1446:skaevo>2.0.co;2.

Wyrtki, K. (1975), EL NINO - DYNAMIC-RESPONSE OF EQUATORIAL PACIFIC OCEAN TO ATMOSPHERIC FORCING, Journal of Physical Oceanography, 5(4), 572-584, doi: 10.1175/1520-0485(1975)005<0572:entdro>2.0.co;2.

Yu, J. Y., C. R. Mechoso, and S. O. C. Amer Meteorol (1997), On the asymmetry of SST in the tropical Pacific, 613-614 pp.

Zebiak, S. E. (1989), OCEANIC HEAT-CONTENT VARIABILITY AND EL NINO CYCLES, Journal of Physical Oceanography, 19(4), 475-486, doi: 10.1175/1520-0485(1989)019<0475:ohcvae>2.0.co;2.

Zhang, X., and J. A. Church (2012), Sea level trends, interannual and decadal variability in the Pacific Ocean, Geophysical Research Letters, 39(21), doi: 10.1029/2012gl053240.

Figure captions

Figure 1. Standard deviation (STD) of sea level anomalies (SLAs, m) of 1993-2016 from (a) AVISO sea level product and (b) HYCOM-CTL. (c) Skewness of SLAs. (d) Regression coefficient k_{Nino} (m) of SLAs onto the normalized Niño-3.4 index for El Niño condition (Niño-3.4 > 0). (e) Same as (b) but for La Niña condition (Niño-3.4 < 0). (f) Ratio of k_{Nino} to k_{Nina}, i.e., $R_k = k_{\mathrm{Nino}}/k_{\mathrm{Nina}}$. SLA data in (c)-(f) are derived from AVISO sea level product of 1993-2016.

Figure 2. R_k distributions during 1993-2016 simulated by (a) HYCOM-CTL, (b) HYCOM-TAU, and (c) RGO-CTL. (d)-(f) are the same as (a)-(c), but for the 1979-2016 period.

Figure. 3. R_k distributions from (a) EXP1, (b) EXP2, (c) EXP1-TAUX and (d) EXP2-TAUX. (e) and (f) show the 1st singular value decomposition (SVD) modes for zonal wind stress τ^x (N m^{-2}; solid and dashed contours for positive and negative values) and upper-layer thickness ULT (m; color shading) of EXP1-TAUX1 for El Niño and La Niña conditions, respectively.

Figure. 4. (a) Zonal structure of the 5°S-5°N average τ^x (left), and ULT (middle) of the 1st SVD mode, and regression coefficients (k_{Nino} and k_{Nina}; right) in EXP1-TAUX, computed separated for the for El Niño and La Niña conditions. (b) Same as (a) but for EXP2-TAUX. (c) is the same as (a), but for τ^x of the 1st SVD mode in RGO-CTL, and theoretically-predicted ULT and regression coefficients (see the text for details), and they are normalized by the standard deviation.

Figures

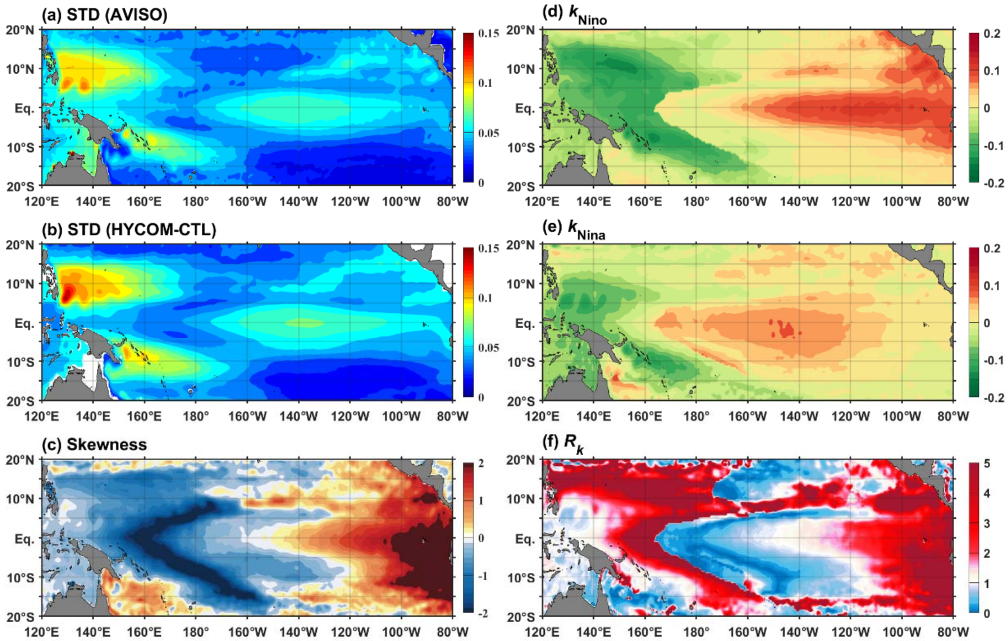

Figure 1. Standard deviation (STD) of sea level anomalies (SLAs, m) of 1993-2016 from (a) AVISO sea level product and (b) HYCOM-CTL. (c) Skewness of SLAs. (d) Regression coefficient k_{Nino} (m) of SLAs onto the normalized Niño-3.4 index for El Niño condition (Niño-3.4 > 0). (e) Same as (b) but for La Niña condition (Niño-3.4 < 0). (f) Ratio of k_{Nino} to k_{Nina}, i.e., $R_{\text{k}} = k_{\text{Nino}}/k_{\text{Nina}}$. SLA data in (c)-(f) are derived from AVISO sea level product of 1993-2016.

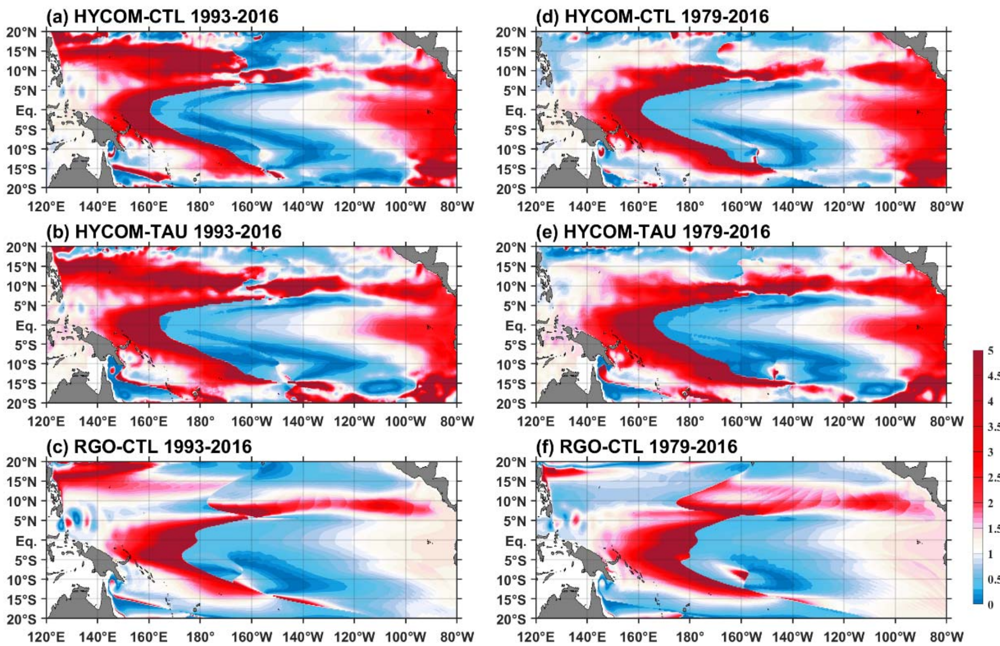

Figure 2. R_k distributions during 1993-2016 simulated by (a) HYCOM-CTL, (b) HYCOM-TAU, and (c) RGO-CTL. (d)-(f) are the same as (a)-(c), but for the 1979-2016 period.

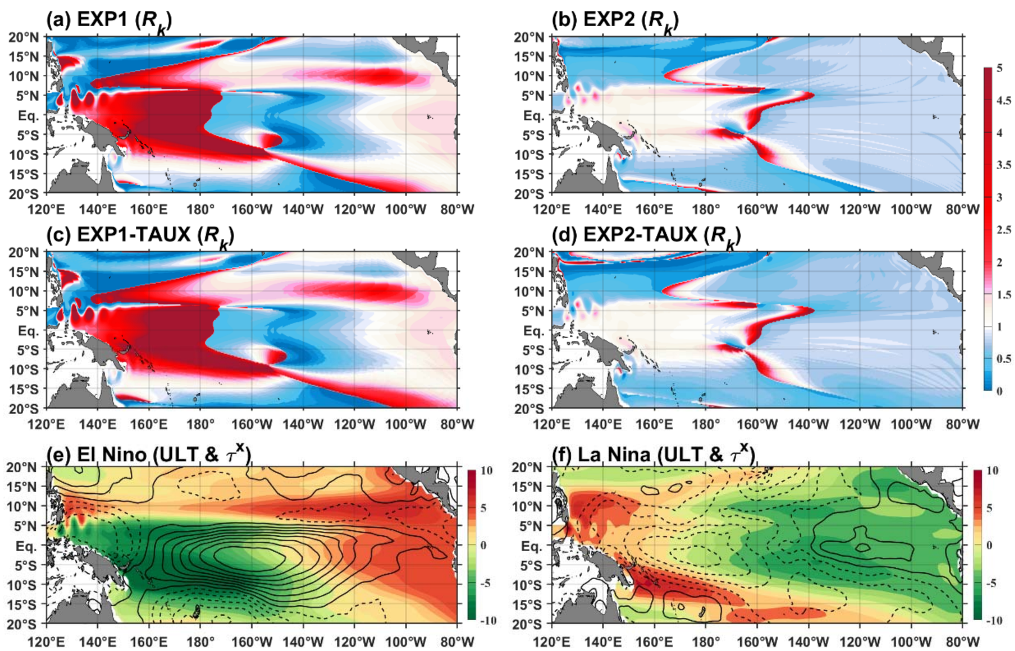

Figure. 3. R_k distributions from (a) EXP1, (b) EXP2, (c) EXP1-TAUX and (d) EXP2-TAUX. (e) and (f) show the 1st singular value decomposition (SVD) modes for zonal wind stress τ^x (N m^{-2}; solid and dashed contours for positive and negative values) and upper-layer thickness ULT (m; color shading) of EXP1-TAUX1 for El Niño and La Niña conditions, respectively.

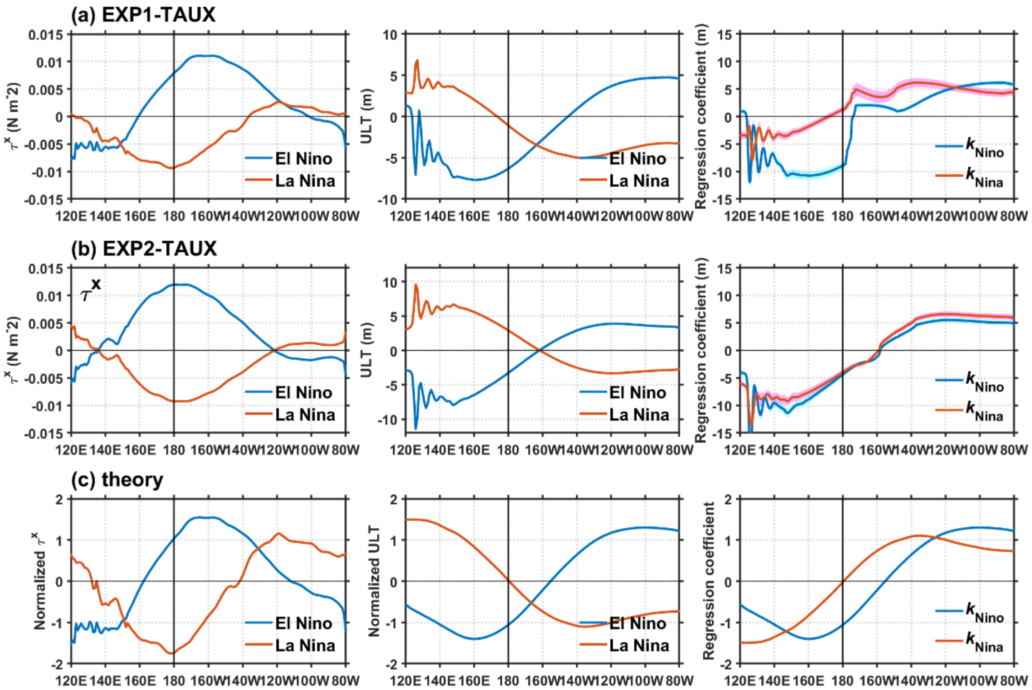

Figure. 4. (a) Zonal structure of the 5°S-5°N average τ^x (left), and ULT (middle) of the 1st SVD mode, and regression coefficients (k_{Nino} and k_{Nina}; right) in EXP1-TAUX, computed separated for the for El Niño and La Niña conditions. (b) Same as (a) but for EXP2-TAUX. (c) is the same as (a), but for τ^x of the 1st SVD mode in RGO-CTL, and theoretically-predicted ULT and regression coefficients (see the text for details), and they are normalized by the standard deviation.